Enhancing Spatial Resolution of Sentinel-2 Next Generation Imagery via Image Fusion

Leonel Garro Linck, Paolo Gamba, *Fellow, IEEE*, and Andrea Garzelli, *Senior Member, IEEE*

***Abstract*—This study presents the analysis of different data fusion techniques to improve the spatial resolution of spaceborne optical images. It was carried out in the context of designing a companion satellite for the Sentinel 2 Next Generation (S2NG) mission, planned to be equipped with either a 2.5 m panchromatic sensor or a three-band multispectral sensor at 2.5 m spatial resolution centered at the red, green, and blue wavelengths. Hence, two primary fusion techniques were investigated: Pansharpening, using a high-resolution panchromatic image, and multisharpening, using a high-resolution multispectral image. To this aim, S2NG test images were synthesized from airborne hyperspectral data. The study explores the effectiveness of both pansharpening, using synthetic panchromatic images, and multisharpening, which directly combines high-resolution RGB with multispectral images. The performance of these techniques was validated using the HQNR index, taking into account both spectral and spatial distortions. In addition, the robustness of these methods against noise and co-registration errors was evaluated. The results indicate that multisharpening provides superior quality enhancement, particularly under varying noise conditions, making it a viable option for future satellite missions requiring high-resolution data fusion.**

***Index Terms*—Image fusion, Sentinel-2, image quality, optical sensor, spatial enhancement.**

I. Scenario and Motivations

THE Sentinel 2 Next Generation (S2NG) is an upcoming satellite mission designed by the European Space Agency (ESA) to continue the legacy of the current Sentinel 2 constellation, providing critical multispectral imagery for various applications [1]. However, the planned S2NG will lack bands with spatial resolution finer than 5 m, presenting a challenge for applications that may require more detailed surface information, such as agricultural parcel mapping, built-up structure characterization, and disaster-related scene analysis.

Received 14 January 2025; revised 30 April 2025 and 19 July 2025; accepted 8 September 2025. Date of publication 11 September 2025; date of current version 22 September 2025. The work of Leonel Garro Linck was supported by the University of Pavia. This work was supported in part by the Italian Ministry for Foreign Affairs and in part by the Italian Space Agency. The work of Paolo Gamba was supported by the "S2NG Scientific Support Study" ESA Project. *(Corresponding author: Paolo Gamba.)*

Leonel Garro Linck is with Instituto de Altos Estudios Especiales Mario Gulich, Universidad Nacional de Córdoba, 5187 Córdoba, Argentina (e-mail: mailto:leonel.garro@ig.edu.ar).

Paolo Gamba is with the Department of Electrical, Biomedical and Computer Engineering, University of Pavia, 27100 Pavia, Italy (e-mail: paolo.gamba@unipv.it).

Andrea Garzelli is with the Department of Information Engineering and Mathematics, University of Siena, 53100 Siena, Italy (e-mail: andrea.garzelli@unisi.it).

Digital Object Identifier 10.1109/JSTARS.2025.3608781

To overcome this limitation, ESA is assessing the launch of a small companion satellite that would fly in formation with S2NG and carry a very high resolution (VHR) imaging payload. Rather than attempting to collect hundreds of narrow hyperspectral bands which would be prohibitive in terms of mass, power, and downlink, the companion satellite would acquire either a single panchromatic band or three broad RGB bands at ground sample distances on the order of a few meters. These VHR images can then be fused with the contemporaneous S2NG multispectral observations, injecting fine spatial detail into the 10–30 m bands while retaining their rich spectral content. This synergy forms the basis for the spatial resolution enhancement methods and the scene simulation framework presented in this work.

To simulate this scenario, our study uses synthetic images generated from two multispectral sensors, Hydice and ROSIS, to represent the data that would be acquired by S2NG and its companion satellite. These synthetic images are adjusted to match the spectral and spatial characteristics expected from the S2NG bands, allowing us to evaluate different data fusion methods in a controlled environment.

The motivation for this work stems from the need to maximize the utility of Sentinel 2 NG satellite data. Enhancing the spatial resolution of multispectral images can significantly improve the accuracy and reliability of various remote sensing applications. By investigating and comparing different data fusion techniques, such as pansharpening and multisharpening, we aim to identify the most effective method for combining high-resolution RGB or panchromatic images with lower-resolution multispectral data.

This article summarizes the following:

1) generates a synthetic benchmark dataset (S2NGRGB/PAN) derived from ROSIS and HyDICE hyperspectral images;
2) compares, for the first time in this context, four classical pansharpening algorithms (OBT, AWLP, GSA, MTFGLPHPMHaze) with two multisharpening schemes (onestep and threestep);
3) evaluates the robustness of each method against additive noise (SNR from 10.3 to 4.3 dB) and coregistration errors up to $\beta = 30°$;
4) demonstrates that the threestep multisharpening scheme outperforms classical methods and supports equipping the companion satellite with a 2.5 m RGB sensor;
5) provides a computational analysis showing that the proposed method is as efficient as the reference algorithms.

II. Related Work

Improving spatial resolution through data fusion involves the integrated processing of two datasets, where at least one is multiband, to create an image that maintains the spectral qualities of the dataset with lower spatial resolution while achieving the spatial resolution of the higher resolution dataset [2]. This procedure, termed pansharpening, specifically refers to cases where the high-resolution dataset is a panchromatic image [3], [4], [5], [6].

Pansharpening is a well-established technique in remote sensing. Pansharpening algorithms have evolved significantly over the years, with various methods developed to balance the tradeoff between spatial and spectral quality [7]. One of the earliest and simplest methods is the Brovey Transform, which integrates the spectral bands with the panchromatic image by maintaining the spectral ratio of the multispectral data [8]. This method, while easy to understand and implement, often results in significant spectral distortions. An optimized version that highly reduces the spectral distortion of the fused image is the Optimized Brovey Transform (OBT) method [9], further improved by a haze-corrected version (OBT-H) [10]. OBT and OBT-H improve on the traditional Brovey Transform by optimizing the weights assigned to each spectral band during the fusion process. This optimization aims to minimize the spectral distortion while enhancing the spatial details.

Another widely used technique is the Gram-Schmidt Spectral Sharpening method, which utilizes the Gram-Schmidt orthogonalization process to decorrelate the multispectral data before merging them with the panchromatic image. Its optimized version, the GS adaptive (GSA) method, has been shown to produce better spectral quality compared to the Brovey Transform [11].

In addition, the additive wavelet luminance proportional algorithm (AWLP) [12] with revised histogram matching [9] provides fully reproducible high performance pansharpening. Similarly, the MTF-GLP-HPM-H method, which adopts the Gaussian Laplacian Pyramid and a high-pass modulation injection model with haze correction, provides high-quality fused products [10].

Recent studies have presented notable examples of Deep Learning-based pansharpening methods, either by training directly at the panchromatic spatial resolution [5] or by effectively leveraging both spatial and spectral information [6].

In cases where a panchromatic image is unavailable or no single sharpening band exists, hypersharpening is used. This technique enhances the less spatially resolved bands by combining the more spatially resolved bands, typically within the visible and near-infrared spectrum [2]. The objective is to maximize the match between the synthesized Pan image formed from the sharpening bands and the lower-resolution band that is being sharpened. This approach takes advantage of shared spatial and spectral patterns.

Initially applied to single-platform data [13], hypersharpening has been extended to multiplatform scenarios [14], [15].

In this article, both pansharpening and hypersharpening (hereafter referred to as *multisharpening*) are tested on simulated images to compare different data fusion methods and support the design and the exploitation of future spaceborne optical sensors. Fig. 1 provide a block diagram illustrating the image fusion process.

TABLE I
Central Wavelengths, Bandwidths, and Spatial Resolutions for Synthetic S2NG and RGB Images

Band	Sentinel 2 - NG			RGB		
	λ (nm)	BW (nm)	Res. (m)	λ (nm)	BW (nm)	Res. (m)
1	408	20	10	432	48	2.5/1.3
2	432	48	30	520	27	2.5/1.3
3	471	29	5	650	17	2.5/1.3
4	484	75	5		—	
5	520	27	10		—	
6	560	44	5		—	
7	620	24	5		—	
8	650	17	5		—	
9	666	37	5		—	
10	695	20	10		—	
11	740	11	10		—	
12	760	12	10		—	
13	782	24	10		—	
14	850	114	5		—	
15	860	13	5		—	
16	960	14	30		—	
17	1000	15	10		—	
18	1350	1	30		—	
19	1620	128	10		—	
20	2200	228	10		—	
21	2112	70	10		—	
22	2142	69	10		—	
23	2237	74	10		—	
24	2264	64	10		—	

III. Methodology

Image Synthesis: In this study, due to the absence of real images from the S2NG satellite and its companion, we used data from available airborne hyperspectral sensors: Hydice and ROSIS 3. The Hydice sensor has 191 bands ranging from 401 to 2473 nm, while ROSIS 3 has 103 bands between 430 and 838 nm. The ROSIS sensor has a spatial resolution of 1.3 m, whereas the Hydice sensor has a spatial resolution of 2.5 m. These hyperspectral images were processed to simulate the different resolutions and wavelengths of S2NG and its companion mission, according to the specifications detailed in Table I.

Specifically, the S2NG bands S_k were synthesized starting from the following spectral synthesis of the hyperspectral bands

$$S_k^{(H)} = \frac{\sum_l H_l G(\lambda_l^{(k)}) \Delta_l^{(k)}}{\sum_l \Delta_l^{(k)}}, \qquad k = 1, \ldots, 24 \tag{1}$$

where H_l is the lth hyperspectral band, $G(\lambda)$ is the spectral response function of S2-NG, $\lambda_l^{(k)}$ the central wavelength of the lth hyperspectral band in the spectral range of the kth S2NG

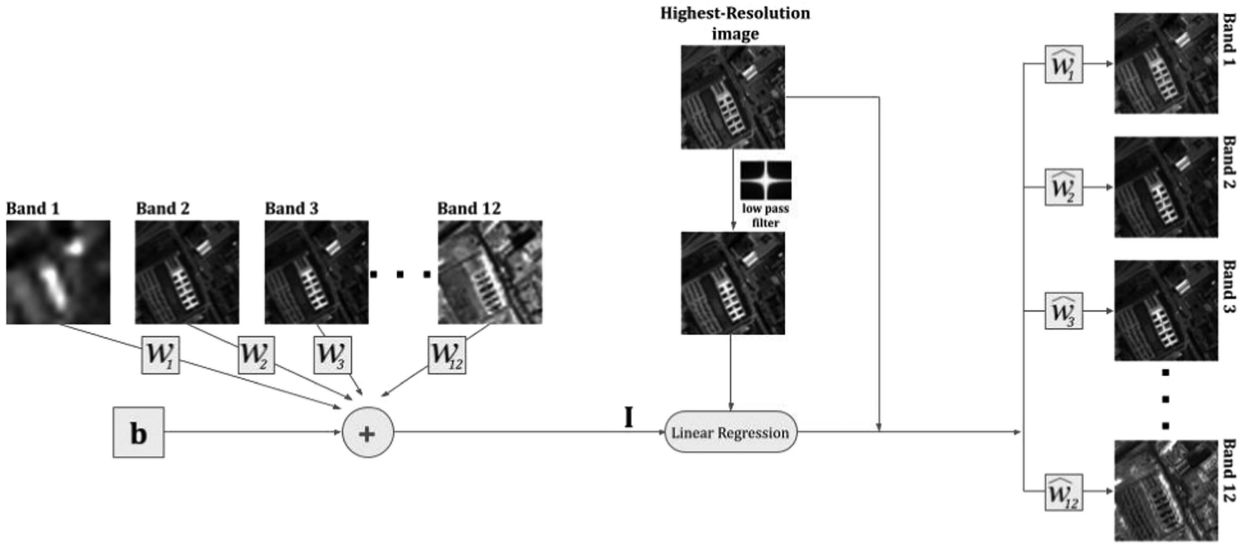

Fig. 1. Diagram illustrating the image fusion process, combining a high-resolution image (PAN or RGB) with a multispectral image to enhance spatial and spectral resolution.

band, and $\Delta_l^{(k)}$ is the wavelength range of the lth hyperspectral band in the spectral range of the kth S2NG band. The S2NG bands S_k are finally obtained by spatially degrading the $S_k^{(H)}$ bands to the corresponding S2NG spatial resolutions reported in Table I.

A. Pansharpening Process

For the pansharpening process, a panchromatic image was obtained in two different ways as follows.

Direct Panchromatic Image: Assuming that the companion satellite for S2NG will be equipped with a panchromatic sensor, a panchromatic image was synthesized from airborne hyperspectral data by applying the relative spectral radiance response of the 503–675 nm panchromatic band of the NASA OLI sensor [16].

Synthetic Panchromatic Image: Under the hypothesis that the companion satellite for S2NG will be equipped with a high resolution RGB sensor, a panchromatic image was synthesized by performing a weighted sum of the three RGB bands ($PAN = w_1R + w_2G + w_3B$), where the weights (w_1, w_2, w_3) were defined considering the standards of the International Commission on Illumination (CIE) [17].

In both cases, the Optimized Brovey Transform (OBT), the Gaussian Laplacian Pyramid with high-pass modulation injection model with haze correction (MTF-GLP-HPM-H), the adaptive Gram-Schmidt (GSA) and the Additive Wavelet Luminance Proportional (AWLP) algorithm were tested.

B. Multisharpening Process

For the multisharpening process, the high-resolution RGB bands were used to improve the spatial resolution of the lower-resolution multispectral image. This process was carried out following two approaches proposed and discussed in [18].

One-Step procedure. The S2NG bands at 5, 10, and 30 m are sharpened by the RGB bands. Each band to be spatially enhanced is sharpened by an optimal linear combination, in the MMSE sense, of the 2.5-m sharpening RGB bands.

Three-Step procedure. The sharpening of the S2NG bands is achieved using MS data that have previously been sharpened: 1) 30-m bands to 10 m; 2) 10-m bands to 5 m using also the enhanced bands from the first step; 3) 5-m bands to 2.5 m using also the enhanced bands from the second step. The number of nested steps is equal to the overall number of different resolutions concerned minus one, i.e., three steps in this case.

C. Validation

To approximate real-world conditions, noise and co-registration errors were added to the images. Additive white Gaussian noise (AWGN) with different levels of signal-to-noise ratio (SNR) was used to model interference. Registration errors were also simulated due to differences in the observation angle between the two sensors and the acquisition geometry of the high-resolution image by the companion satellite.

The validation of the results was performed exploiting the Hybrid Quality with No Reference (HQNR) index, which evaluates the spatial and spectral distortions of the fused images [19]. The HQNR index is a no-reference quality assessment method, which means that it does not require a reference image to evaluate the quality of the fused image. This is particularly useful in remote sensing applications where reference images are often unavailable. The HQNR index considers two primary types of image distortion: 1) spatial distortion (D_S), which reflects the loss of spatial details in the fused image compared to the target high-resolution image and 2) spectral distortion ($D_\lambda^{(F)}$), which indicates the loss of spectral information due to the fusion process.

The HQNR index is meant to consider both distortions and its basic formula is as follows:

$$\text{HQNR} = (1 - D_\lambda^{(F)}) \times (1 - D_s). \tag{2}$$

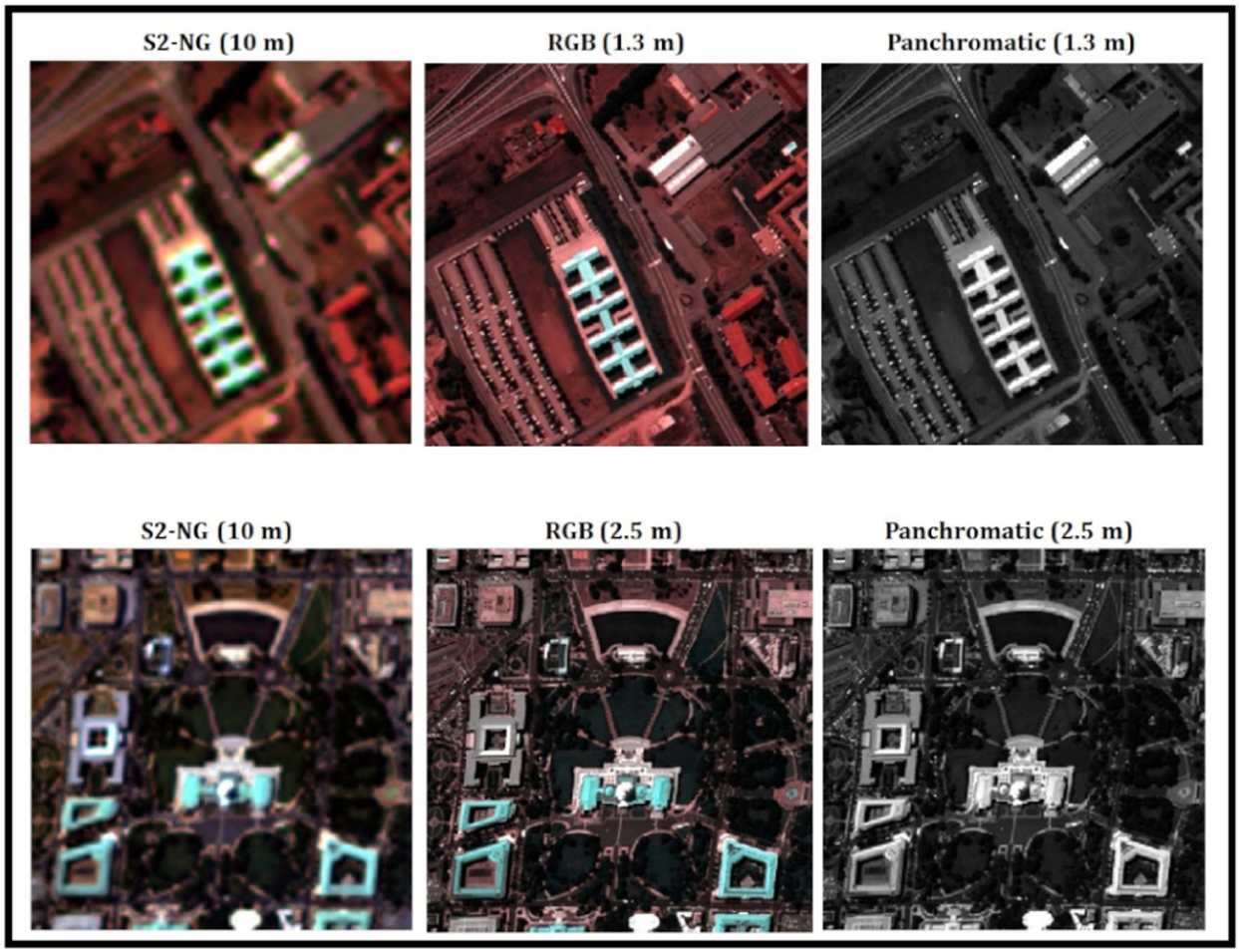

Fig. 2. Synthesized B16-B7-B4 S2NG images obtained from the hyperspectral images of the ROSIS (top) and Hydice (bottom) sensors.

A HQNR value close to 1 indicates high-quality fused images, which means that the fusion process has effectively preserved both spatial and spectral details. D_s and $D_\lambda^{(F)}$ are given by the following equations, as expressed in [19]:

$$D_s = \frac{1}{N_\lambda} \sum_{i=1}^{N_\lambda} |Q(\widetilde{M}_i, P_L) - Q(\widehat{M}_i, P)| \tag{3}$$

$$D_\lambda^{(F)} = 1 - Q2^n(\widehat{M}_{L\downarrow}, M) \tag{4}$$

where N_λ is the number of spectral bands in the multispectral image M, $\widehat{M}$ is the fused image, $\widehat{M_{L\downarrow}}$ the fused image degraded to the original spatial resolution of M, and P and P_L denote the panchromatic image and its low-pass filtered version, respectively. $Q(a, b)$ is the Universal Image Quality Index (UIQI) between single-band images a and b, which was originally proposed in [20], and $Q2^n(A, B)$ is its generalization for 2^n multiband images A and B [21].

IV. Experimental Results

A. Experimental Setup

To compare the different options for pansharpening and multisharpening, simulated images were generated from two hyperspectral sensors, Hydice and ROSIS 3, since real satellite images with S2NG characteristics were unavailable. The Hydice image is formed by 191 bands ranging from 401 nm to 2473 nm, while the ROSIS 3 sensor dataset includes 103 bands, from 430 to 838 nm. The image obtained by ROSIS depicts the engineering campus of the University of Pavia, while the image obtained by the Hydice sensor is about the city of Washington, DC. The spatial resolution of the ROSIS sensor is 1.3 m, while the spatial resolution of the Hydice sensor is 2.5 m. These hyperspectral images were adjusted to match the various resolutions and bands outlined in Table I, aligning with the characteristics that both the S2NG and its companion will have.

For both pansharpening and multisharpening methods, the spatial resolution of the high-resolution image is initially reduced using a low-pass filter. Subsequently, a linear regression algorithm is applied to the multispectral S2NG bands to compute the weights that minimize the mean squared error between the spatially degraded sharpening image and the multispectral S2NG bands to be enhanced.

Fig. 2 reports the synthesized images generated from the hyperspectral sensors. Note that the images from the S2NG sensor have bands with spatial resolutions of 5, 10, and 30 meters. The depicted images have a resolution of 10 m, since they represent color compositions of bands 4, 7, and 16, all of which have a resolution of 10 m.

TABLE II
HQNR VALUES FOR DIFFERENT NOISE CONDITIONS

	HQNR	
SNR (dB)	**One Step**	**Three Steps**
10.3	0.95	0.95
7.7	0.92	0.92
6.2	0.83	0.89
5.1	0.72	0.85
4.3	0.63	0.81

B. Multisharpening Strategy: One-Step and Three-Step

In multisharpening, high-resolution RGB images were fused with multispectral images through linear regression and considering different bands for regression calculation. Two methods were tested: 1) the one-step method, which calculates weights for each band individually to enhance the bands directly to 2.5 m for Hydice (or to 1.3 m for ROSIS 3); 2) and the three-step method, which applies a nested scheme to the S2NG bands from 30 to 10 m, from 10 to 5 m, and finally to the highest resolution (2.5 or 1.3 m). The Quality Index (HQNR) was used to validate the results, considering both spatial and spectral distortions. HQNR values close to 1 indicate better performance. The two methods showed similar HQNR values under standard conditions, but the three-step method demonstrates greater robustness under increased noise conditions, as shown in Table II.

The multisharpening results were assessed through the HQNR protocol, which showed that despite the added noise and misregistration errors, the three-step method consistently performed better, suggesting its suitability for future applications in enhancing Sentinel 2 NG imagery.

With this analysis, we conclude that the most efficient method is the so-called three-step method referred to as multisharpening.

C. Noise and Misregistration Errors

To introduce noise and misregistration errors for more realistic scenarios, AWGN was applied to the high-resolution RGB images, with SNR levels ranging from 10.3 to 4.3 dB.

Considering that the orbital parameters of the companion satellite will be the same as those of Sentinel 2-NG, the differences in image co-registration will arise from the fact that the footprint of the companion satellite is significantly smaller than that of Sentinel 2. Specifically, the design anticipates that the former will have a footprint of 30 km, while Sentinel 2 has an approximate footprint of 190 km (Fig. 3). With these considerations, for the companion satellite to capture an image of the boundaries of the Sentinel 2 footprint, it will need to adjust its inclination by an angle of up to 27°. In Fig. 4, the image distortion is shown due to this difference in observations. Coregistration errors were introduced by creating a transformation matrix that included both a rotation angle and an error due to the image deformation caused by the angle of view of the satellite (β).

After applying this distortion, an automatic tool was utilized to realign the images. This tool compares the original and distorted images and performs an inverse transformation to correct

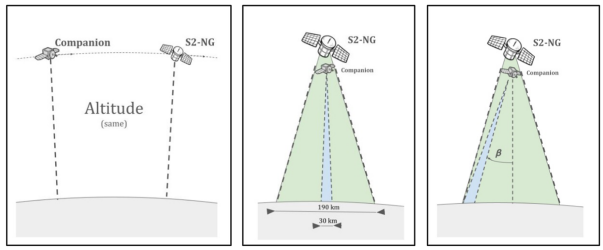

Fig. 3. Illustration of the Sentinel-2 NG and its companion satellite configuration. (Left) Both satellites operate at the same altitude. (Center) Swath difference: Sentinel-2 NG covers 190 km, while the companion satellite covers 30 km. (Right) Angular offset (β) between the acquisition geometries, which introduces distortion in the image.

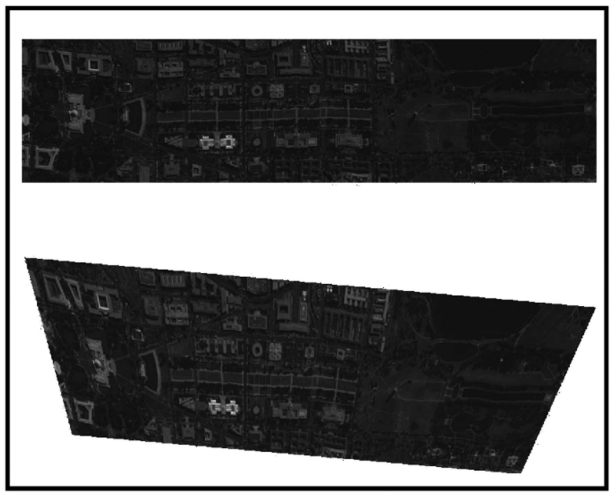

Fig. 4. Original image (above) and image distorted by an exaggerated viewing angle (below).

the misalignment. The effectiveness of this correction process was then assessed by analyzing the quality of the corregistered images

$$A1 = \begin{pmatrix} 1+\arctan(\beta) & 0 & 0 \\ \arctan(\beta) & 1 & 0 \\ 0.0017 \cdot \arctan(\beta) & 0 & 1 \end{pmatrix} \tag{5}$$

$$A2 = \begin{pmatrix} \cos\theta & -\sin\theta & 0 \\ \sin\theta & \cos\theta & 0 \\ 0 & 0 & 1 \end{pmatrix} \tag{6}$$

$$A = A2 \cdot A1 = \begin{pmatrix} \cos\theta & -\sin\theta & 0 \\ \sin\theta & \cos\theta & 0 \\ 0 & 0 & 1 \end{pmatrix} \begin{pmatrix} 1+\arctan(\beta) & 0 & 0 \\ \arctan(\beta) & 1 & 0 \\ 0.0017 \cdot \arctan(\beta) & 0 & 1 \end{pmatrix}. \tag{7}$$

In this transformation matrix, the angle θ represents the rotation angle of the sensed image, and the factor $A1$ corresponds to the distortion due to the viewing angle. Fig. 4 shows an image distorted with an angle of 15° and a distortion angle of 30°.

TABLE III
HQNR VALUES FOR EACH TECHNIQUE UNDER THE DIFFERENT STUDIED CONDITIONS

Technique	Type	NN, ND	LN, ND	LN, LD	LN, HD	HN, LD	HN, HD
Multisharpening	RGB	**0.98**	**0.98**	**0.93**	**0.94**	**0.93**	0.89
OBT	PAN	0.88	0.87	0.87	0.86	0.85	0.83
	RGB	0.90	0.89	0.89	0.82	0.86	0.80
AWLP	PAN	0.92	0.92	0.90	0.89	0.89	0.87
	RGB	0.91	0.91	0.89	0.83	0.87	0.80
GSA	PAN	0.95	0.94	0.92	0.91	0.92	**0.90**
	RGB	0.95	0.94	0.92	0.86	0.91	0.83
MTF-GLP-HPM-Haze	PAN	0.95	0.94	0.85	0.65	0.83	0.62
	RGB	0.95	0.94	0.75	0.27	0.78	0.27

The abbreviations represent the following conditions: NN (No Noise), ND (No Distortion), LN (Low Noise, SNR = 43dB), HN (High Noise, SNR = 15dB), LD (Low Distortion, distortion angle $\beta = 5^{\circ}$), and HD (High Distortion, distortion angle $\beta = 30^{\circ}$).

These values are significantly larger than in a practical scenario, but are included to illustrate the method.

Having defined the methods for introducing errors due to both noise and coregistration, we proceeded to test the various methods with these variations on high-resolution images (RGB images for multisharpening and PAN images for pansharpening). Nine different techniques were compared: Multisharpening using the RGB image, and eight pansharpening methods, including OBT, AWLP, GSA, and MTF-GLP-HPM-Haze, applied to both panchromatic (PAN) and RGB images (with a synthetic PAN generated).

To evaluate these techniques, the HQNR index values of the resulting images were analyzed under six distinct conditions: NN, ND (No Noise, No Distortion); WN, ND (With Noise, No Distortion); LN, LD (Low Noise, Low Distortion); LN, HD (Low Noise, High Distortion); HN, LD (High Noise, Low Distortion); and HN, HD (High Noise, High Distortion). The results for each technique and condition are summarized in Table III.

The first observation from this comparison is that the highest HQNR index values are achieved using the multisharpening technique, for both the ROSIS and Hydice sensors. In addition, for all techniques, the HQNR index values are consistently higher for the synthesized images derived from the Hydice sensor data. This can be attributed to the lower spatial resolution of the Hydice sensor compared to the ROSIS sensor (2.5 m versus 1.3 m, respectively). Consequently, the spatial resolution improvement, that is, the scale ratio, required for the ROSIS images is greater, thereby imposing a higher demand on the algorithms.

When comparing the two pansharpening methods, it is evident that using RGB images to synthesize the PAN image yields similar HQNR indices initially when no errors are added to the images. However, when errors due to noise or coregistration are introduced, the synthesized PAN image from the RGB data demonstrates greater stability to these variations. This leads to the conclusion that, if pansharpening is to be employed, it would be more advantageous to utilize a high-resolution RGB image.

Given that our satellite will provide information on the angles at which images are captured, allowing for the correction of images prior to fusion, we can infer that the coregistration error has less influence than the noise error in satellite images during the image fusion process. Therefore, analyzing the behavior of different methods in the presence of varying noise levels is a fundamental aspect of this study.

To this end, we generated high-resolution images with different noise levels and compared the HQNR quality index values for each result. The findings of this analysis are presented in Figs. 5 and 6.

As seen in the data presented in Table II, the values of the HQNR quality index in Table III are consistently higher when the multisharpening technique is applied. Furthermore, when comparing pansharpening methods, the technique using RGB images is more efficient than directly using the panchromatic image. However, it is also evident that as noise levels increase, the HQNR values for multisharpening decrease more significantly than those for pansharpening. This observation suggests that in scenarios with high noise level, GSA pansharpening with the RGB image may be more advantageous.

TABLE IV
COMPUTACIONAL TIMES: RELATIVE PERCENTAGE AND EFFECTIVE EXECUTION TIME (MULTISHARPENING TIME: 2.97 S)

	RGB (s)	PAN (s)	RGB (%)	PAN (%)
OBT	1.45	1.36	105%	118%
AWLP	1.99	2.03	49%	46%
MTF	1.64	1.59	81%	87%
GSA	1.55	1.53	92%	94%

D. Computational Costs

Table IV presents both the absolute runtimes for each fusion algorithm (based on RGB or PAN) and their relative execution times, expressed as a percentage of the multisharpening baseline. The reference time for multisharpening is 2.97 s, measured on a $600 \times 216 \times 103$ image using a MATLAB implementation on an Intel i7 processor. The results demonstrate the efficiency of the multisharpening technique, with execution times comparable to those of classical pansharpening algorithms.

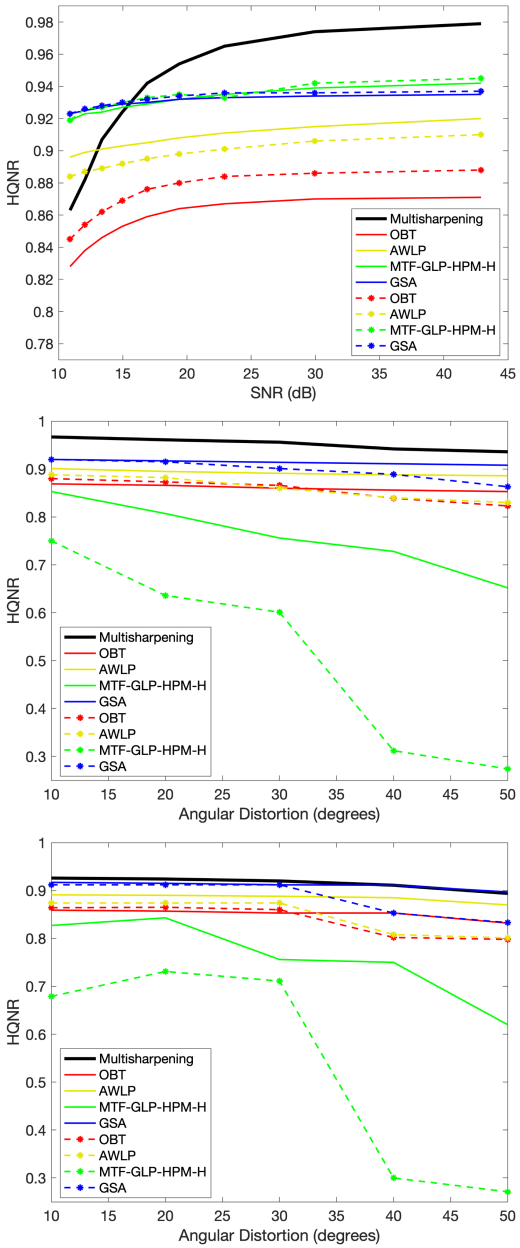

Fig. 5. HQNR index results for the HyDICE sensor. The first plot shows the HQNR index as a function of the SNR in the absence of distortion. The second and third plots present HQNR values for different distortion angles, considering a fixed SNR of 40 and 17 dB, respectively. Dashed lines represent the functions obtained with RGB images, while solid lines correspond to those obtained directly with the panchromatic image. The thick black plot shows the multisharpening case.

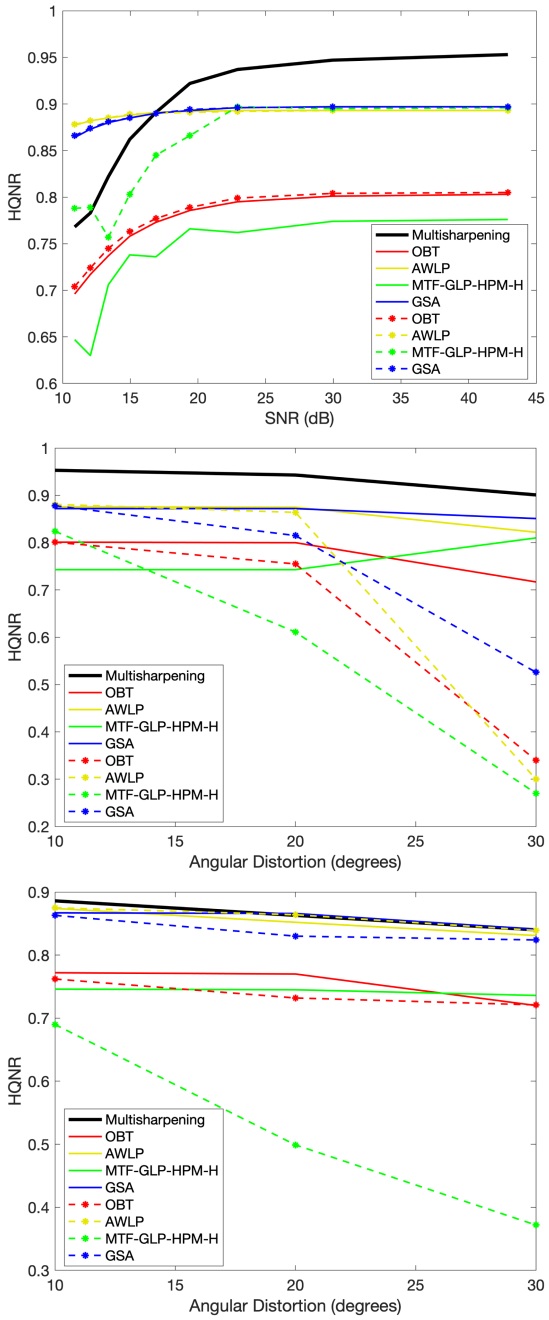

Fig. 6. HQNR index results for the ROSIS sensor. The first plot shows the HQNR index as a function of the SNR in the absence of distortion. The second and third plots present HQNR values for different distortion angles, considering a fixed SNR of 40 and 17 dB, respectively. Dashed lines represent the functions obtained with RGB images, while solid lines correspond to those obtained directly with the panchromatic image. The thick black plot shows the multisharpening case.

E. Visual Comparison

A visual comparison among the different sharpening methods is finally reported in Fig. 7. For each method, a distortion map D is defined as

$$D = \frac{1}{24}\sum_{k=1}^{24}\left[\widehat{S}_k - S_k^{(H)}\right]^2 \tag{8}$$

where $\widehat{S}_k$ is the kth sharpened band and S_k is the corresponding reference band obtained from (1).

As shown in Fig. 7, the multisharpening distortion map exhibits substantially lower spectral deviations than those of the other methods, a difference that is immediately apparent upon visual inspection. All maps have been normalized using the same global range (0 to 1) to ensure direct comparability: 0 corresponds to dark blue and 1 to red. Consequently, the multisharpening map remains predominantly dark blue (indicating

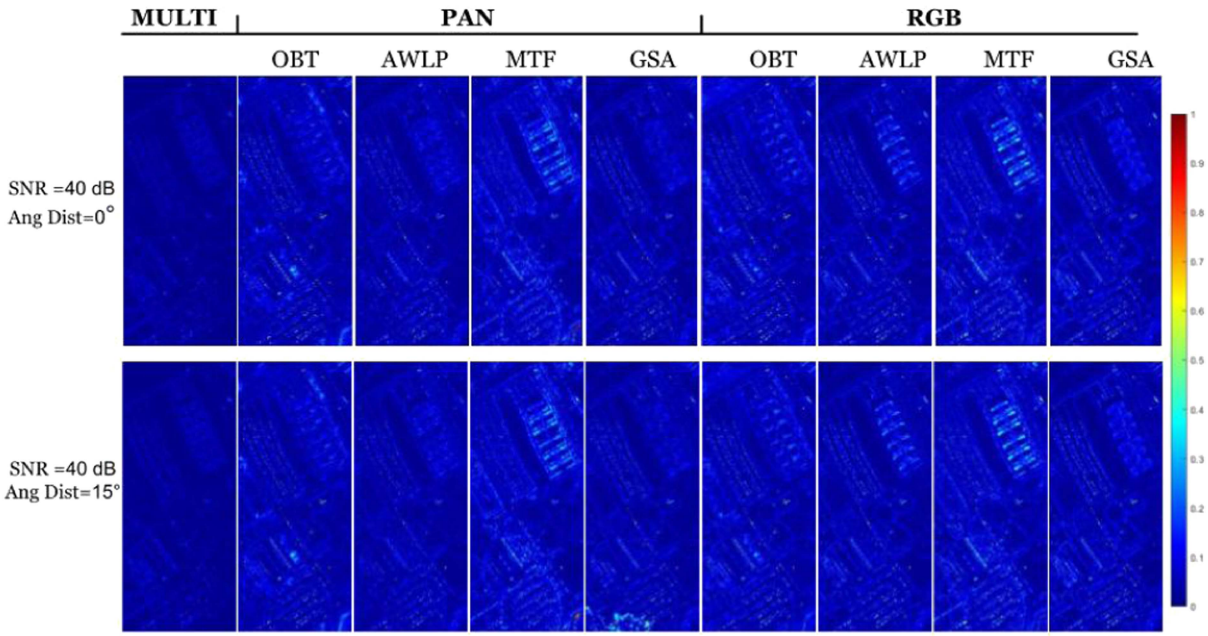

Fig. 7. Visual comparison of normalized distortion maps D for each sharpening method (see main text for definition). The multisharpening method exhibits noticeably lower distortion than the other techniques.

minimal spectral difference) while the other methods, though still mostly blue, display occasional lighter patches in localized regions, reflecting higher spectral discrepancies.

V. Conclusion

This study demonstrates the efficacy of advanced data fusion techniques in enhancing the S2-NG imagery. By comparing pansharpening and multisharpening methods, we have identified the strengths and limitations of each approach in the context of Sentinel-2 NG's mission requirements.

Our experimental results indicate that multisharpening consistently outperforms pansharpening, especially in scenarios involving noise and coregistration errors. The three-step multisharpening method, in particular, has shown robust performance under varying conditions, making it a reliable choice for future applications. The ability of this method to maintain high-quality spatial and spectral information despite external distortions underscores its potential to improve S2-NG imagery.

Furthermore, the HQNR protocol has proven to be an effective metric for evaluating the quality of the fused images, providing a comprehensive assessment of both spatial and spectral characteristics. The use of synthetic data from the Hydice and ROSIS sensors has allowed a controlled evaluation environment, ensuring that the findings are relevant and applicable to real-world scenarios involving S2-NG data.

In the context of designing a companion satellite for Sentinel-2 NG, the results of this study suggest a change in the typical sensor configuration. Traditionally, high-resolution panchromatic bands have been favored for pansharpening processes. However, given the superior performance of multisharpening, it may be more advantageous to equip the companion satellite with a high-resolution RGB sensor instead. This approach eliminates the need for an ultrahigh-resolution panchromatic band, thereby simplifying satellite design while still enabling the desired improvements in spatial resolution.

In addition, the study highlights the potential benefits of using high-resolution RGB data in conjunction with multispectral images. This approach not only enhances spatial resolution, but also leverages the spectral richness of RGB data, which can be critical for applications that require detailed surface information. Therefore, the integration of high-resolution RGB sensors could represent a significant advancement in satellite imaging technology, providing more accurate and reliable data for applications such as land cover mapping, urban planning, and environmental monitoring.

Future research should focus on further refining the multisharpening techniques and exploring their applicability to other satellite missions and sensor configurations. Furthermore, the development of automated tools for real-time image fusion and correction could enhance the operational efficiency and accuracy of satellite imaging systems. A detailed discussion on atmospheric interference would go well beyond the main objectives of the present work. However, this aspect is indeed relevant and will require further investigation for future developments and subsequent studies. In continuing to innovate in this field, it is possible to significantly enhance the capabilities of remote sensing technologies, providing more detailed and accurate data for a wide range of scientific and practical applications.

REFERENCES

[1] P. Martimort et al., "On-going and planned mission concept studies for the preparation of future ESA earth observation satellites," in *Proc. 2023 IEEE Int. Geosci. Remote Sens. Symp.*, 2023, pp. 4582–4585.

[2] L. Alparone, A. Arienzo, and A. Garzelli, "Spatial resolution enhancement of vegetation indexes via fusion of hyperspectral and multispectral satellite data," *Remote Sens.*, vol. 16, no. 5, pp. 875-1–875-21, Mar. 2024.

[3] G. Vivone et al., "A new benchmark based on recent advances in multispectral pansharpening: Revisiting pansharpening with classical and emerging pansharpening methods," *IEEE Geosci. Remote Sens. Mag.*, vol. 9, no. 1, pp. 53–81, Mar. 2021.

[4] G. Vivone, A. Garzelli, Y. Xu, W. Liao, and J. Chanussot, "Panchromatic and hyperspectral image fusion: Outcome of the 2022 WHISPERS hyperspectral pansharpening challenge," *IEEE J. Sel. Top. Appl. Earth Observ. Remote Sens.*, vol. 16, pp. 166–179, 2023.

[5] M. Ciotola, S. Vitale, A. Mazza, G. Poggi, and G. Scarpa, "Pansharpening by convolutional neural networks in the full resolution framework," *IEEE Trans. Geosci. Remote Sens.*, vol. 60, 2022, Art. no. 5408717.

[6] S. Zhang, L. Qiao, F. Zhang, C. Xu, S. Zhao, and Q. Gao, "Spatial-spectral dual guided network with joint attention for pansharpening," *IEEE Trans. Geosci. Remote Sens.*, vol. 63, 2025, Art. no. 5405516.

[7] A. Arienzo, G. Vivone, A. Garzelli, L. Alparone, and J. Chanussot, "Full-resolution quality assessment of pansharpening: Theoretical and hands-on approaches," *IEEE Geosci. Remote Sens. Mag.*, vol. 10, no. 3, pp. 2–35, Sep. 2022.

[8] A. R. Gillespie, A. B. Kahle, and R. E. Walker, "Color enhancement of highly correlated images-II. channel ratio and "chromaticity" transform techniques," *Remote Sens. Environ.*, vol. 22, no. 3, pp. 343–365, Aug. 1987.

[9] L. Alparone, A. Garzelli, and G. Vivone, "Intersensor statistical matching for pansharpening: Theoretical issues and practical solutions," *IEEE Trans. Geosci. Remote Sens.*, vol. 55, no. 8, pp. 4682–4695, Aug. 2017.

[10] S. Lolli, L. Alparone, A. Garzelli, and G. Vivone, "Haze correction for contrast-based multispectral pansharpening," *IEEE Geosci. Remote Sens. Lett.*, vol. 14, no. 12, pp. 2255–2259, Dec. 2017.

[11] B. Aiazzi, S. Baronti, and M. Selva, "Improving component substitution pansharpening through multivariate regression of MS pan data," *IEEE Trans. Geosci. Remote Sens.*, vol. 45, no. 10, pp. 3230–3239, Oct. 2007.

[12] X. Otazu, M. González-Audícana, O. Fors, and J. Núñez, "Introduction of sensor spectral response into image fusion methods. application to wavelet-based methods," *IEEE Trans. Geosci. Remote Sens.*, vol. 43, no. 10, pp. 2376–2385, Oct. 2005.

[13] M. Selva, L. Santurri, and S. Baronti, "On the use of the expanded image in quality assessment of pansharpened images," *IEEE Geosci. Remote Sens. Lett.*, vol. 15, no. 3, pp. 320–324, Mar. 2018.

[14] X. Lu, J. Zhang, X. Yu, W. Tang, T. Li, and Y. Zhang, "Hyper-sharpening based on spectral modulation," *IEEE J. Sel. Top. Appl. Earth Observ. Remote Sens.*, vol. 12, no. 5, pp. 1534–1548, 2019.

[15] R. Restaino, G. Vivone, P. Addesso, and J. Chanussot, "Hyperspectral sharpening approaches using satellite multiplatform data," *IEEE Trans. Geosci. Remote Sens.*, vol. 59, no. 1, pp. 578–596, Jan. 2021.

[16] Julia A. Barsi, Brian L. Markham, and Jeffrey A. Pedelty, "The operational land imager: Spectral response and spectral uniformity," in *Earth Observing Systems XVI*, J. J. Butler, X. Xiong, and X. Gu, Eds., vol. 8153, Bellingham, WA, USA: International Society for Optics and Photonics, 2011, Art. no. 81530.

[17] ITU-R, "Recommendation BT.709-6: Parameter values for the HDTV standards for production and international programme exchange," *Radiocommunication Sector, Int.* Telecommunication Union, Geneva, 2015, last accessed, Sept. 13, 2025, [Online]. Available: https://www.itu.int/dms_pubrec/itu-r/rec/bt/R-REC-BT.709-6-201506-I!!PDF-E.pdf

[18] L. Alparone, A. Arienzo, and A. Garzelli, "Spatial resolution enhancement of satellite hyperspectral data via nested hyper-sharpening with Sentinel-2 multispectral data," *IEEE J. Sel. Topics Appl. Earth Observ. Remote Sens.*, vol. 17, pp. 10956–10966, 2024.

[19] B. Aiazzi, L. Alparone, S. Baronti, R. Carlà, A. Garzelli, and L. Santurri, "Full-scale assessment of pansharpening methods and data products," in *Image and Signal Processing for Remote Sensing XX*, L. Bruzzone, Ed., vol. 9244, Bellingham, WA, USA: SPIE, 2014, pp. 1–12.

[20] Z. Wang and A. C. Bovik, "A universal image quality index," *IEEE Signal Process. Lett.*, vol. 9, no. 3, pp. 81–84, Mar. 2002.

[21] A. Garzelli and F. Nencini, "Hypercomplex quality assessment of multi-/hyper-spectral images," *IEEE Geosci. Remote Sens. Lett.*, vol. 6, no. 4, pp. 662–665, Oct. 2009.

Leonel Garro Linck received the Licenciatura in physics and the Ph.D. degree in physics from the National University of Córdoba (UNC), Argentina, in 2016 and 2021, respectively. His Ph.D. dissertation focused on nuclear magnetic resonance of confined liquids in porous media.

He is a Research Fellow with the University of Pavia, Italy, working on Earth observation and remote sensing within the Department of Industrial and Information Engineering (Dip. Ingegneria Industriale e dell'Informazione). He previously served as a Lecturer of optics with the Instituto Universitario Aeronáutico, Córdoba, Argentina. His research interests include hyperspectral imaging, data fusion, and space systems applications.

Paolo Gamba (Fellow, IEEE) received the Laurea degree in Electronic Engineering "cum laude" from the University of Pavia, Italy, in 1989, and the Ph.D. degree in electronic engineering from the same University in 1993. He is Professor at the University of Pavia, Italy in the Telecommunications and Remote Sensing Laboratory. He served as Editor-in-Chief of the IEEE Geoscience and Remote Sensing Letters from 2009 to 2013 and of the IEEE Geoscience and Remote Sensing Magazine in 2023-2024. He was Chair of the Data Fusion Committee of the IEEE Geoscience and Remote Sensing Society (GRSS) from 2005 to 2009. He has been elected in the GRSS AdCom from 2014 to 2022 and served as GRSS President from 2019 to 2020. He also served as Technical Co-Chair of the 2010, 2015, and 2020 IGARSS conferences, in Honolulu (Hawaii), Milan (Italy), and on-line, respectively. He is Fellow of IEEE, IAPR, AAIA and the Academia Europaea. He has been invited to give keynote lectures and tutorials on several occasions about urban remote sensing, data fusion, EO data for physical exposure and risk management. He published more than 210 papers in international peer-review journals.

Andrea Garzelli (Senior Member, IEEE) received the "Laurea" degree (summa cum laude) in electronic engineering and the Ph.D. degree in information and telecommunications engineering from the University of Florence, Italy, in 1991 and 1995, respectively.

He has coauthored the book *Remote Sensing Image Fusion* (CRC Press, 2015). He is a Professor of telecommunications with the Department of Information Engineering and Mathematics, University of Siena, Italy. He holds the courses of fundamentals of signal processing and telecommunications, statistical signal processing, and remote sensing with the same university. His research interests include image analysis and classification with applications to image fusion for optical and synthetic aperture radar images.

He was a co-recipient of the GEOSCIENCE AND REMOTE SENSING LETTERS Prize Paper Award in 2004. He received recognition as one of the Best Reviewers of IEEE TRANSACTIONS ON GEOSCIENCE AND REMOTE SENSING in 2014, a journal for which he has been an Associate Editor since 2015.Since 2019, he has been consistently listed in Stanford University's ranking of the World's Top 2% Scientists, both for each individual year and for his entire career.